velopment Vehicles," TN D-1396, Dec. 1962, NASA.
Barnes, D. R., "Analysis of Dynamics of Mother-Daughter Rocket Separation Systems," NASA CR 55153, 1963, Penn State Univ. Ionosphere Research Lab., University Park, Penn.
Abbot, H. M., "Bibliography-Separation and Ejection Systems of Flight Vehicles," SB 64-14, July 1964, Lockheed Missiles & Space Co., Sunnyvale, Calif.
Narahara, R. M., "Computer-Aided Design," *Space/Aeronautics*, Vol. 52, No. 7, Dec. 1969, pp. 56–58.

APRIL 1970 J. SPACECRAFT VOL. 7, NO. 4

Computer Analysis of Complex Shell Structures

DAVID BUSHNELL*
Lockheed Palo Alto Research Laboratory, Palo Alto, Calif.

A digital computer program for the general analysis of composite ring-stiffened shells of revolution is used for the analysis of two typical liquid-propellant rocket nozzle configurations. The program, called BOSOR3, is briefly described. It is then shown how the mathematical models of the nozzles are constructed. These nozzles are of complex wall construction and are submitted to internal pressure, axial compression, and bending. In the analysis the nozzles are treated as segmented, longitudinally stiffened, orthotropic layered shells. A stress analysis and a stability analysis are performed for each of the two nozzle configurations. Comparisons with the test results are given. The predicted failure load and mode agree well with those observed in the test. It is determined that both nozzle configurations are stress-critical, failure of the wall material first occurring just aft of the throat in the outer fibers of the wall.

Nomenclature

A = cross section area, in.^{2}
e_1,e_2 = radial, axial distances from reference surface (coolant pipe centerline) to discrete ring centroid, in.
E = Young's modulus, psi
G = shear modulus, psi
I = moment of inertia, in.^{4}
J = torsion constant, in.^{4}
L = distance from point of application of lateral load S to end B of nozzle (Fig. 2)
$\bar{M}$ = effective moment at nozzle throat ($\bar{M} = 51S$), in.-lb
M_{10} = meridional moment resultant, positive for compressive stress in outer fiber at $\theta = 0$, in.-lb/in.
N_{10},N_{20} = meridional, circumferential stress resultants, positive for tension, lb/in.
n = number of circumferential waves
p = chamber pressure, psi
Q = transverse applied shear load/length, lb/in.
r = radius from centerline to reference surface, measured normal to axis of revolution, in.
S = lateral load (Fig. 2), lb
s = arc length measured from clamped end A
t = thickness, in.
$T(2)$ = distance from centroid of coolant pipes to wire windings, in.
T = axial thrust, positive compression, lb
u,v,w = meridional, circumferential, normal displacement components, in.
V = axial load/length, lb/in.
x,y = axes attached to discrete rings (Fig. 4b)
z = axial distance along nozzle, in.
λ = Lagrange multiplier
θ = circumferential coordinate
χ = rotation of meridian in its plane
ν = Poisson's ratio

Subscripts

B = value at end B of nozzle (Fig. 2)
i = mesh point number
p = pertaining to coolant pipes
t = value at nozzle throat
0 = prebuckling quantity
1,2 = meridional and circumferential directions, respectively
12 = twist or shear

Received January 30, 1969; revision received November 19, 1969. This research was sponsored by the Aerojet-General Corporation, Sacramento, Calif.

* Staff Scientist, Aerospace Sciences Laboratory. Member AIAA.

Introduction

Tests on Liquid-Propellant Nozzles

FIGURE 1 shows a nozzle for a liquid-propellant rocket that was tested under combined static loads at the Aerojet-General Corporation in Sacramento, Calif.[1] The nozzle consists of steel coolant pipes which run in the meridional direction. These pipes form a layer of the nozzle wall, which is reinforced by steel wire wound circumferentially over portions of the surface and by a number of discrete ring stiffeners. The test nozzle with applied loads is sketched in Fig. 2. It is clamped at A and bolted to a cylinder at B. The cylinder is free to translate and rotate as a rigid body. The static lateral load S simulates a transient bending moment caused primarily by forces imposed upon the nozzle by the inertia of its aft skirt during ignition and initial firing of the engine.

Three tests were performed on the nozzle shown in Fig. 1. In the first test the chamber was pressurized to 700 psi and a maximum compressive thrust load $T = 10{,}230$ lb was applied in increments and then removed. A maximum shear load $S = 1000$ lb was then applied in increments and removed, after which the chamber was returned to zero pressure. The coolant pipes were pressurized to 1000 psi throughout this test. No damage was sustained by the nozzle. In the second test brittle lacquer (Stresscoat) was applied to the exterior throat. After the coolant pipes and the chamber had been pressurized to 1000 and 700 psi, respectively, a maximum thrust load of 43,000 lb was applied in increments and held. An indicated shear load of 1200 lb was then applied in increments. The loads and pressures were removed and the chamber inspected. The actual applied shear load, corrected for pin friction and side component of thrust, amounted to about 1000 lb during this run. There was no apparent damage. In the third test the loading sequence was the same

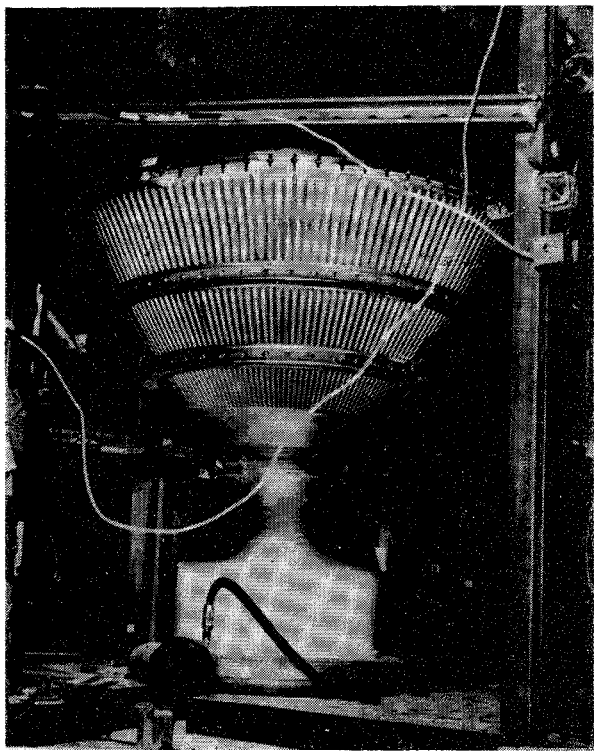

Fig. 1 Test nozzle in test rig (courtesy Acrojet General, Sacramento, Calif.).

as that just decribed, except that the shear load S was applied in increments until the nozzle failed at approximately S = 1800 lb. Failure appeared to be imminent at S = 1600 lb, since the chamber deformed steadily at this load level. Cracks appeared in the brittle lacquer during the yielding process, indicating an axial strain level of at least 2000 μin./in. just aft of the throat at the outer fibers on the compression side. The chamber failed suddenly, apparently when the wire windings gave way. Figure 3 shows a closeup of the damaged area just aft of the throat. The failure was apparently caused by excessive axial compressive stresses in the region where circumferential cracks appear. This failure at S = 1600 to 1800 lb motivated an effort to design a stronger nozzle.

The purpose of this paper is to predict the failure of the test configuration (henceforth referred to as the test nozzle) and to obtain similar data for the new, stronger design configuration (henceforth referred to as the design nozzle). Each configuration is essentially a shell structure with a rather complex wall construction consisting of a layer of tubes for regenerative cooling reinforced by various types of wire winding and ring stiffeners (Figs. 4a–4c). The static loads applied to the test nozzle (Fig. 2) simulate static and dynamic loads which are present during ignition and initial firing of the engine. These forces could cause the nozzle structure to fail by local yielding or by general instability below or above the elastic limit. It is necessary, therefore, to calculate the loads that cause initial yielding in the wall material and to determine whether the nozzles buckle.

The BOSOR3 Computer Program

The BOSOR3 computer program[2] was used for the stress and stability analyses of the nozzles. This program is a general shell of revolution analyzer for complex ring-stiffened segmented shells with various types of wall construction. Other computer programs have also been written for the analysis of shells of revolution. In his computer analysis Cohen[3] uses a step-by-step numerical integration technique to calculate buckling loads of ring-stiffened orthotropic shells of revolution. Kalnins[4] employs a similar method to calculate nonsymmetric deformations of segmented shells of revolution submitted to nonsymmetric loads. Percy, Pian, Klein, and Navaratna[5] use the finite-element method for the linear stress analysis of general shells of revolution. Navaratna, Pian, and Witmer[6] extend the analysis of Ref. 5 to treat buckling of shells of revolution. The work of Refs. 5 and 6 led to a series of computer programs under the name SABOR. The latest program in this series, SABOR4, is documented in Ref. 7.

The BOSOR3 program[2] is very general with respect to the type of analysis which it will perform. Depending on the value of a control integer, the program will calculate axisymmetric stresses and displacements from a nonlinear theory for a series of step-wise increasing thermal or mechanical loads; will determine critical loads corresponding to axisymmetric collapse; will determine buckling loads corresponding to nonsymmetric buckling modes for a range of circumferential wave numbers, seeking the minimum load; will calculate vibration frequencies of prestressed shells corresponding to axisymmetric and nonsymmetric modes; and will calculate displacements and stresses in nonsymmetrically loaded shells. The program can be used for the analysis of ring-reinforced, layered, orthotropic, longitudinally stiffened shells submitted to various combinations of axisymmetric and nonsymmetric mechanical and thermal distributed and line loads. In this paper the two nozzle configurations fall into this category.

The assumptions upon which the BOSOR3 code is based are: 1) The material is elastic. 2) Thin shell theory is valid, that is, normals to the undeformed surface remain normal and undeformed. 3) The structure is axisymmetric, and in buckling and vibration analyses and nonlinear stress analysis the loads and prebuckling or prestress deformations are axisymmetric. 4) The prebuckling deflections, while considered finite, are moderate. That is, the square of the meridional rotation can be neglected compared to unity. 5) In the calculation of displacements and stresses in nonsymmetrically loaded shells, linear theory is used. This branch of the program is based on standard small-deflection analysis. 6) The discrete ring stiffeners are reasonably thin. That is, a typical cross section dimension is small compared to the radius of the ring. 7) The cross sections of the rings remain undeformed during the deformations of the structure, and the rotation about the ring centroid is equal to the rotation of the shell meridian at the attachment point of the ring. 8) The ring centroids coincide with the ring shear centers. 9) If meridional stiffeners are present, they are numerous enough to include in the analysis by an averaging or smearing of their properties over any parallel circle of the shell structure.

The coefficients of the constitutive equations and details of their derivation are given in Refs. 2 and 8. The wall properties can vary along the meridian. A structure composed of many segments can be analyzed, and the properties of each shell segment are independent of those of the other segments.

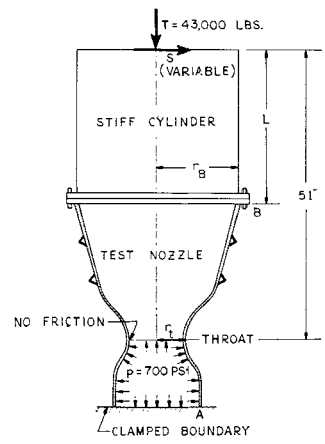

Fig. 2 Test nozzle as loaded in static test.

With regard to boundary conditions, any displacement components and the meridional rotation can be specified zero, or other boundary conditions can be simulated by introduction of support rings at the edges.

The BOSOR3 program represents the codification of three distinct analyses. 1) A nonlinear stress analysis for axisymmetric behavior of axisymmetric shell systems. 2) A linear stress analysis for axisymmetric and nonsymmetric behavior of axisymmetric shell systems submitted to axisymmetric and nonsymmetric loads. 3) An eigenvalue analysis in which the eigenvalues represent buckling loads or vibration frequencies of axisymmetric shell systems submitted to axisymmetric loads (eigenvectors may correspond to axisymmetric or nonsymmetric modes).

An energy formulation is used in conjunction with the method of finite differences. An algebraic form for the total potential and kinetic energy of the system is derived through extensive use of matrix algebra. The development is similar to that used in the finite element method, and is ideally suited for programming on the digital computer. Other investigators[9–11] have also based their analyses on energy minimization in which the displacement derivatives appearing in the kinematic relations are replaced by appropriate finite difference forms.

The independent variables of the analysis are the arc length, s, measured along the shell reference surface and the circumferential coordinate, θ. The dependent variables are the displacement components u, v, and w of the shell wall reference surface. The numerical analysis is based on the finite difference method, so that in the computer program the dependent variables are the displacement components u_i, v_i, and w_i at discrete points (mesh points) on the shell reference surface.

For the three analyses listed previously it is possible to eliminate the circumferential coordinate θ by separation of variables: in the nonlinear axisymmetric stress analysis θ is not present; in the linear stress analysis the nonsymmetric load system is expressed as a sum of harmonically varying quantities, the shell response to each harmonic being calculated separately; and in the eigenvalue analysis the eigenvectors vary harmonically around the circumference. Thus, the θ-dependence (where applicable) is eliminated by the assumption that $u(s,\theta)$, $v(s,\theta)$, $w(s,\theta)$, are given by $u_n(s)\sin n\theta$, $v_n(s)\cos n\theta$, $w_n(s)\sin n\theta$ or by $u_n(s)\cos n\theta$, $v_n(s)\sin n\theta$, $w_n(s)\cos n\theta$. In the BOSOR3 analysis the first three harmonically varying displacement components correspond to values $n > 0$; the last three to $n \leq 0$.

The analysis is based on energy minimization with constraint conditions. The total energy of the system involves strain energies of the shell segments U_s and the discrete rings U_r, potential energy of the applied line loads and pressures U_p, and kinetic energies of the shell segments T_s and the discrete rings T_r. The constraint conditions U_c arise from 1) displacement conditions at the ends of the composite shell and 2) compatibility conditions between adjacent segments of the composite shell. These components of energy and the constraint conditions are initially integro-differential forms. They are then written in terms of the shell reference surface displacement components u_i, v_i, and w_i at the finite-difference mesh points and Lagrange multipliers, λ_i. The integration is performed numerically by the trapezoidal rule. Now an algebraic form, the energy is minimized with respect to the discrete dependent variables.

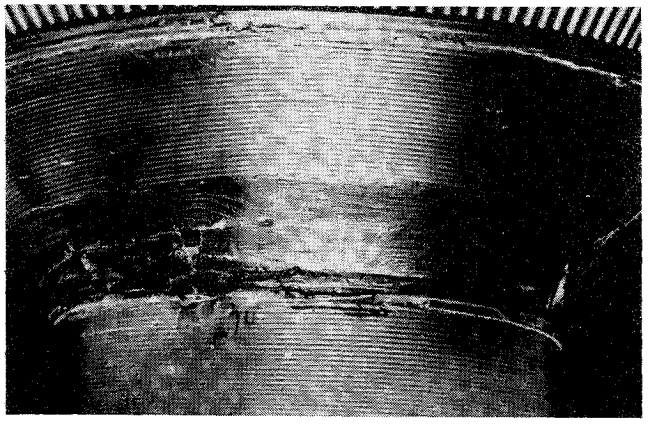

Fig. 3 Test nozzle after failure under combined chamber pressure p, axial thrust T, and lateral load S (courtesy Aerojet General, Sacramento, Calif.).

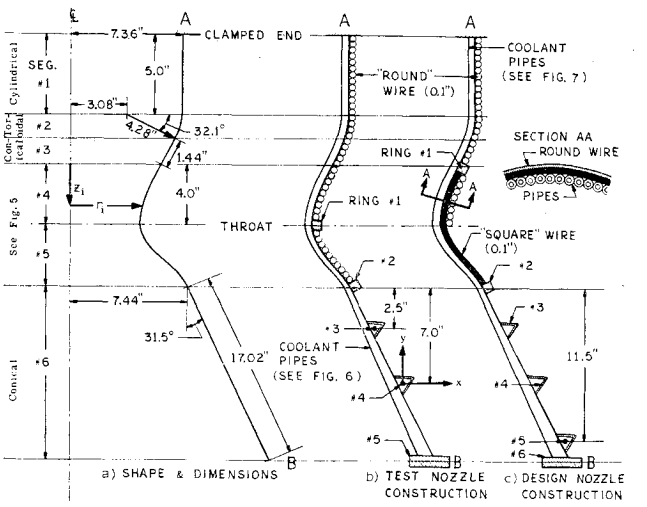

Fig. 4 Meridional geometry and wall construction of test and design nozzles.

In the nonlinear stress analysis the energy expression has terms linear, quadratic, cubic, and quartic in the dependent variables. The cubic and quartic terms arise from the "rotation-squared" terms which appear in the constraint conditions and in the kinematic expressions for reference surface strains ϵ_1, ϵ_2, and ϵ_{12}. Energy minimization leads to a set of nonlinear algebraic equations which are solved by the Newton-Raphson method. Stress and moment resultants are calculated in a straightforward manner from the mesh point displacement components through the constitutive equations (stress-strain law) and kinematic (strain-displacement) relations.

The results from the nonlinear axisymmetric stress analysis are used in the eigenvalue analyses for buckling and vibration. The prebuckling or prestress meridional and circumferential stress resultants N_{10} and N_{20} and the meridional rotation χ_0 appear as known variable coefficients in the energy expression which governs buckling and vibration. This expression is a homogeneous quadratic form. The values of a parameter (load or frequency) which render the quadratic form stationary with respect to infinitesimal variations of the dependent variables represent buckling loads or natural frequencies. These eigenvalues are calculated from a set of linear, homogeneous equations.

The same linear stability equations, with a right-hand-side vector added, are used for the linear stress analysis of axisymmetrically and nonsymmetrically loaded shells. The right-hand-side vector represents load terms and terms due to thermal stress. The variable coefficients, N_{10}, N_{20}, and χ_0, mentioned above are zero of course since there is no nonlinear prestress analysis. Further details of the analysis are given in Refs. 2 and 12.

Models

Geometry

Two nozzle configurations are analyzed for stress and stability: the test nozzle and the stronger design nozzle. Figure 4 shows a) the meridian shape of both nozzles, b) the wall

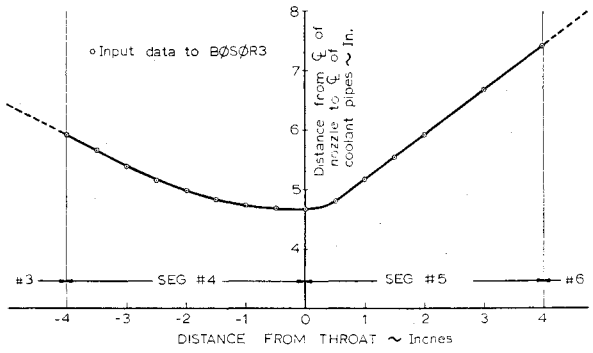

Fig. 5 Geometry of meridian in segments 4 and 5.

construction of the test nozzle, and c) the wall construction of the design nozzle. The dimensions in Fig. 4a refer to the centerline of the coolant pipes. These pipes form a layer of the nozzle wall which is reinforced by 0.1-in.-diam steel wire wound circumferentially over portions of the surface. Some of the wire has a circular cross section and some has a square cross-section. The design nozzle is stronger than the test nozzle by virtue of thicker coolant pipes, the addition of wire windings with square cross section, and the addition of a discrete ring near the aft end B. The meridian geometry of the throat region (segments 4 and 5) is given in Fig. 5, the coolant pipe dimensions for the test nozzle are given in Fig. 6, and those for the design nozzle are given in Fig. 7. The meridian geometry of the throat region is supplied to the BOSOR3 program as points (z_i, r_i) in a cartesian frame. The program calculates derivatives of r and the meridional and normal circumferential curvatures from the (z_i, r_i) input by means of a spline fit method.

The nozzles are brazed so that the wire and pipes form a shell wall which is assumed to obey the Kirchoff-Love hypothesis (normals remain normal), and to remain intact throughout the loading and initial buckling processes. In the aft portion of the nozzles (portion with no wire reinforcement) the pipes are brazed and the structure is reinforced by steel V-bands as shown in Figs. 4b and 4c. These bands are treated as discrete elastic rings in the analysis. The aft ends B of the nozzles are assumed to be supported by very stiff steel rings and the forward ends A are assumed to be clamped. The properties of the discrete ring stiffeners for the test nozzle and design nozzle are listed in Table 1. These properties are referred to x-y centroidal axes such as shown associated with Ring 4 in Fig. 4b.

Wall Properties

The wall construction of the two nozzles is shown in Fig. 4. The nozzles are analyzed as if composed of layers which are reinforced by meridional stiffeners. Each layer in the mathematical model of the wall is orthotropic. The properties of the layers corresponding to the round and square wire windings are listed in Table 2, which applies to both nozzles. The pipes are represented as an orthotropic layer with the meridional modulus $E_1 = 0$, reinforced by meridional stiffeners. This layer is located a distance $T(2)$ from the layers corresponding to the wire windings. The hoop and shear moduli for the pipe layer (Layer No. 1) are given by

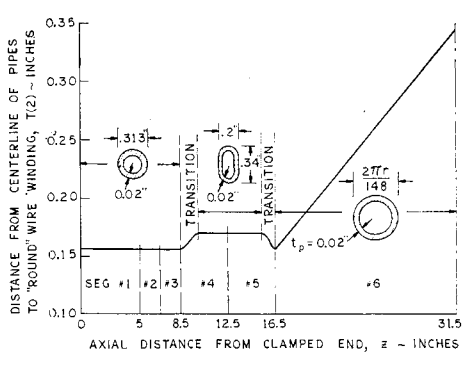

Fig. 6 Coolant pipe geometry for test nozzle.

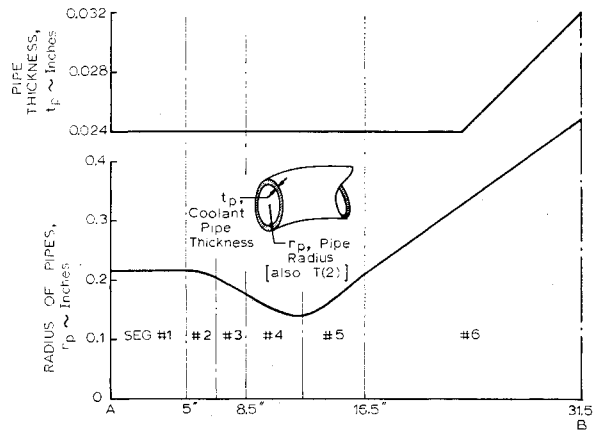

Fig. 7 Coolant pipe geometry for design nozzle.

$$E_2 = 9/\pi\,(r_p/t_p)(E(t_p/r_p)^3/12(1-\nu^2) + p_p/4) \quad (1)$$

$$G_p = G\pi/2 \quad (2)$$

in which t_p is the pipe wall thickness, r_p is the pipe radius, p_p is the coolant pressure, and E is the modulus of the pipe wall material. Equation (1) is easily derived from an approximate analysis of the inextensional deformation of an infinite pressurized thin cylinder submitted to two diametrically opposed line loads distributed uniformly along opposite generators. Corresponding to E_2 the effective thickness of the pipe layer is t_p. The effective shear modulus of the pipe wall G_p is needed for the nonsymmetric elastic stability analysis. If the effective thickness is taken as t_p, it can be shown from Ref. 13 that Eq. (2) gives the effective shear modulus, in which G is the shear modulus of the pipe wall material.

In the case of the design nozzle, the pipes have circular cross sections, and there are 114 of them forming a complete circumference. Therefore, $r_p = \pi r/114$, where r is the radius of the nozzle measured to the centerline of the pipes. The meridional modulus of the pipe layer is assumed to be zero, since the meridional rigidity is accounted for by the introduction of stiffeners with cross section area, moment of inertia, and torsion constant given by,

$$A_p = 2\pi r_p t_p, \quad I_p = \pi r_p^3 t_p, \quad J_p = 2I_p \quad (3)$$

In the case of the test nozzle there are 148 pipes. These have circular cross-sections everywhere except in the neighborhood of the throat, where they are oblong in cross section (see Fig. 6). In this case two parameters are needed to describe the geometry: the radius of the ends of the oblong, still denoted r_p; and the depth of the oblong, half of which represents the distance $T(2)$ between the centerline of the pipes and the innermost windings. In the computer program this distance is read in as $T(2)$, denoting thickness of the second layer. The radius $r_p = \pi r/148$. Equations (3) are retained for the properties of the meridional stiffeners, with the radius r_p replaced by the distance $T(2)$. This is admittedly an approximation in the vicinity of the throat, albeit a good one considering the close approximation of A_p and I_p. Equations (1) and (2) are used as is. Figure 6 shows the axial distribution of $T(2)$. The pipe thickness t_p is constant and equal to 0.02 in. By thus combining the orthotropic layer with the meridional stiffeners, one accounts in a reason-

Table 1 Geometry properties of steel rings for test and design nozzles

Ring no.	Radius to centroid, in.	Cross section area, in.^{2}	Moments of inertia, 10^{-4} in.^{4} I_y	I_x	I_{xy}	Eccentricities, in. e_1	e_2	Torsional stiffness GJ, 10^5, lb-in.^{2}
Test nozzle [see Fig. 4b]								
1	4.955	0.095	4.95	11.4	0.0	0.275	0	0
2	7.636	0.0722	4.51	6.35	−3.12	0.196	−0.147	0
3	10.62	0.096	79.8	30.01	48.98	0.637	−0.391	2.21
4	13.25	0.096	79.8	30.01	48.98	0.718	−0.441	2.21
5	16.35	1.415	0.686	0.259	0.421	0	0	0
Design nozzle [see Fig. 4c]								
1	6.15	0.0775	2.9	1.14	−1.8	0.212	0.133	0
2	7.68	0.0500	1.07	0.598	0.8	0.240	−0.179	0
3	10.62	0.096	79.8	30.01	48.98	0.637	−0.391	2.21
4	13.25	0.096	79.8	30.01	48.98	0.718	−0.441	2.21
5	15.88	0.096	79.8	30.01	48.98	0.804	−0.493	2.21
6	16.35	1.415	0.686×10^4	0.259×10^4	0.421×10^4	0	0	0

ably accurate way for the essential characteristics of a sheet which is composed of pipes brazed together along generators.

Once the properties of each layer are determined, the properties of the composite wall are calculated as described in Ref. 8. The properties of the nozzle wall at a typical station where all layers are present are listed in Table 2. Note that layer 2 is simply a spacer; it has infinite transverse shear stiffness only. The meridional modulus for the round wire layer $E_1 = 7.03 \times 10^6$ psi is derived from a formula given by Roark[14] for the deformation of two solid cylinders submitted to diametrically opposed loads. Inclusion of this meridional stiffness of the round wire has a rather large effect on the predicted critical applied shear load S. The test results reported in Ref. 1 seem to justify the assumption that the round wire helps to support the nozzle on the compression side.

Loading

The axisymmetric loads (chamber pressure $p = 700$ psi and axial thrust $T = 43{,}000$ lb) are applied as shown in Fig. 2. The thrust T is considered to act at the end B of the nozzle. The lateral shear S applied 51 in. aft of the throat is modeled as a bending moment plus shear acting at B. The bending moment is replaced by an axial load/length $V = (SL/\pi r_B^2)\cos\theta$, in which L and r_B are shown in Fig. 2, and $\theta = 0$ corresponds to the compression side of the nozzle. The shear load is considered to be distributed uniformly over the circumference at B, so that loads/length normal to the shell Q and circumferentially tangent N_{12} are given by $Q = (S/2\pi r_B)\cos\theta$ and $N_{12} = -(S/2\pi r_B)\sin\theta$. In the linear stress analysis the chamber pressure p and thrust T give an axisymmetric ($n = 0$) stress distribution, and the loads V, Q, and N_{12} give a nonsymmetric stress distribution with one circumferential wave ($n = -1$, see discussion of BOSOR3 analysis). The total stress due to the load combination shown in Fig. 2 is obtained by superposition of the $n = 0$ and $n = -1$ modes.

Table 2 Properties of shell wall at typical station where all layers are present

Layer no. (inner layer first)	Thickness, in.	Moduli, 10^6 psi Shear	E_1	E_2	Poisson's ratio, ν_{12}
1 (Equivalent to pipes)	t_p (Figs. 6, 7)	G_p Eq. (2)	0	E_2 Eq. (1)	0
2 (Spacer)	$T(2)$ (Figs. 6, 7)	0	0	0	0
3 ("Square" wire)	0.1 (0 for test nozzle)	11.5	30	30	0.3
4 ("Round" wire)	0.079 (Equivalent thickness for round wire with 0.1 in. diam)	11.5	7.03	30	0.3

The above discussion pertains to the stress analysis of the nozzles. In the stability analysis it is necessary because of limitations of the BOSOR3 computer program to establish an axisymmetric model of the load system. Since the throat area appears to be critical, the axisymmetric model is set up such that the maximum compressive stresses near the throat are hopefully reasonably accurate. The axisymmetric model is checked in the next section by comparison with the more accurate model used for the prediction of stress.

For the stability analysis an axisymmetric axial load V is established at B which yields the same maximum axial compressive load/length at the throat as that obtained from a statically determinate membrane theory analysis of the nozzle shown as loaded in Fig. 2. For example, with $S = 1$ lb in Fig. 2 the bending moment $\bar{M}$ at the throat is 51 in./lb. This moment is equilibrated by an axial load/length at the throat $V_t = (\bar{M}/\pi r_t^2)\cos\theta$, in which r_t is the throat radius shown in Fig. 2. If this axial load/length were considered to act axisymmetrically it would correspond to an axisymmetric axial load/length at B given by $V_B = \bar{M}/(\pi r_t r_B)$, or in terms of S: $V_B = 51S/(\pi r_t r_B)$. This load V_B represents the eigenvalue parameter in the stability analysis. The chamber pressure p and axial thrust T are held constant and represent fixed system parameters which affect the stiffness matrix of the stability analysis in a known way (see Ref. 2).

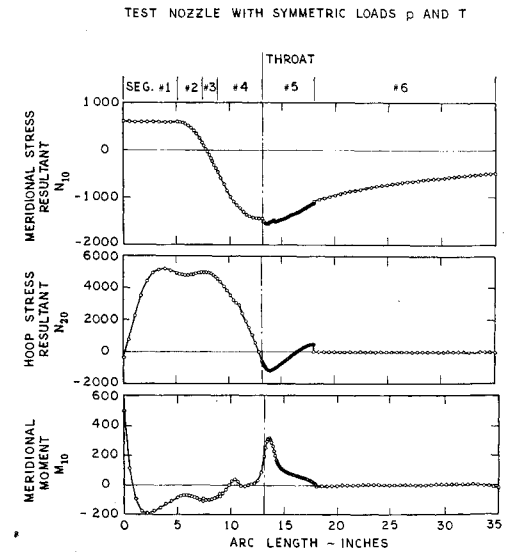

Fig. 8 Stress and moment resultants for test nozzle loaded by chamber pressure $p = 700$ psi and axial thrust $T = 43{,}000$ lbs.

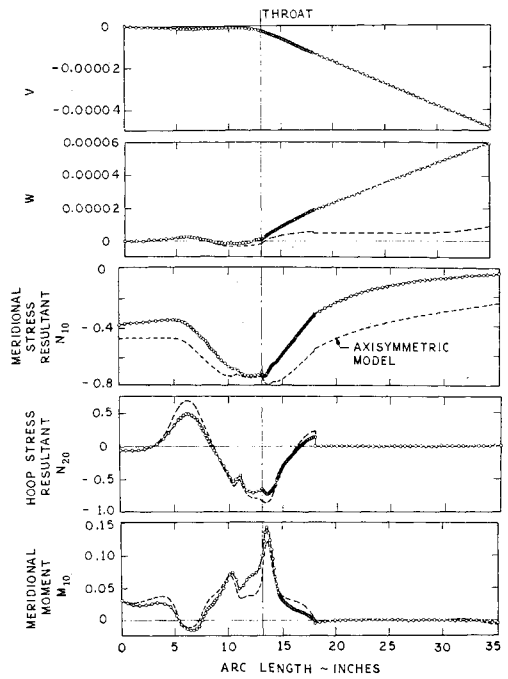

Fig. 9 Displacements and stress resultants for test nozzle submitted to a lateral load S = 1 lb, applied 51 in aft of throat.

Theoretical Results

Some runs on the Univac 1108 computer were made to determine the optimum distribution of finite-difference mesh points and the most favorable division of the nozzles into segments. As a result the nozzles were divided into six segments as shown in Fig. 4. The mesh points were distributed as follows: 10 points in segment 1; 10 points in segment 2; 10 points in segment 3; 15 points in segment 4; 44 points in segment 5; and 36 points in segment 6. Points are concentrated in the segment corresponding to the region just aft of the throat, since the test nozzle failed initially at a location about 0.5 in. aft of the throat. Typical run times for a stress analysis are about 10–20 sec. For a complete stability analysis, including nonlinear prebuckling effects, about 60 sec are required on the Univac 1108.

Stress Analysis

Figure 8 shows SC-4020 plot output generated by BOSOR3. These data correspond to the test nozzle loaded only by the chamber pressure p = 700 psi and axial thrust T = 43,000 lb. The arc length is measured in inches along the reference surface from the clamped end. Division of the shell into six segments is shown. The maximum compressive stresses, both meridional and hoop, occur in the outer fiber about $\frac{1}{2}$ in. aft of the throat. The sign convention of the meridional moment resultant M_{10} is such that a positive moment corresponds to compression in the outer fiber.

The solid lines in Fig. 9 show the test nozzle displacement components v and w and stress and moment resultants N_{10}, N_{20}, and M_{10} corresponding to a lateral shear load S of 1 lb applied 51 in. aft of the throat. This load is modeled as described in the first paragraph of the section with subhead "Loading." All other applied loads are zero. The quantities w, N_{10}, N_{20}, and M_{10} correspond to $\theta = 0$, which is the meridian with the greatest axial compression, and v corresponds to $\theta = 90°$. From the plots of v and w it is seen that the motion of the nozzle under the lateral shear load S can roughly be described as a rigid-body rotation of the aft portion of the nozzle about a point near the throat. (If the stiff ring at B moves as a rigid body, the circumferential displacement v at $\theta = 90°$ would be given by $v = -[w\cos(31.5°) + u\sin(31.5°)]$ or in this case $v = -4.846 \times 10^{-5}$ in. The calculated value from BOSOR3 is -4.823×10^{-5} in.) The curvature of the area in the immediate neighborhood of the throat changes significantly with increasing shear load S, a phenomenon which leads to the peak in the bending moment distribution, M_{10}. This peak coincides with the peak compressive stress resultant N_{10} and with the peak values of N_{10} and M_{10} corresponding to the test nozzle loaded by chamber pressure p and axial thrust T (Fig. 8). It appears likely that this reinforcing peaking of all the axial compressive stress quantities caused the failure of the test nozzle. The critical stress is located in the outer fiber just aft of the throat. Similar results are obtained for the design nozzle.

Figure 10 shows maximum compressive meridional and hoop stresses for the test and design nozzles plotted as functions of the bending moment $\bar{M} = 51\,S$ at the throat. Zero bending moment $\bar{M}$ corresponds to the nozzles loaded by a chamber pressure of 700 psi plus an axial compressive thrust of 43,000 lb. Initial yielding occurs when the outer fiber stresses reach about 45,000 psi. The hoop stresses are calculated with the assumptions that the hoop strain is constant through the wall thickness and only the windings carry the stress resultant N_{20}. These approximations are reasonable since the contribution of the hoop stiffness of the pipes is small compared to that of the windings. In the design nozzle the effective hoop modulus of the pipes at the throat is 1.33×10^6 psi with an effective thickness of 0.024 in. and in the test nozzle the effective hoop modulus of the pipes at the throat is 0.920×10^6 psi with an effective thickness of 0.020 in. [See Eq. (2)].

It is seen from Fig. 10 that inclusion of the meridional stiffness E_1 of the round wire has a significant effect on the prediction of the compressive stress at the outer fiber of the pipes in the test nozzle. That these windings absorbed stress on the compression side during the test is evident, since the brittle lacquer Stress-coat cracked during the yielding process—indicating an axial strain level of at least 2000 μin./in. just aft of the throat.

General Instability

It is necessary to show conclusively that the test nozzle did not fail because of general instability in the elastic range and that the design nozzle will not so fail. The theory developed in Ref. 2 is used to calculate bifurcation buckling loads for both nozzles. The wall material is assumed to remain elastic. The stability analysis on which the BOSOR3 program is based is limited to axisymmetrically loaded structures, even though

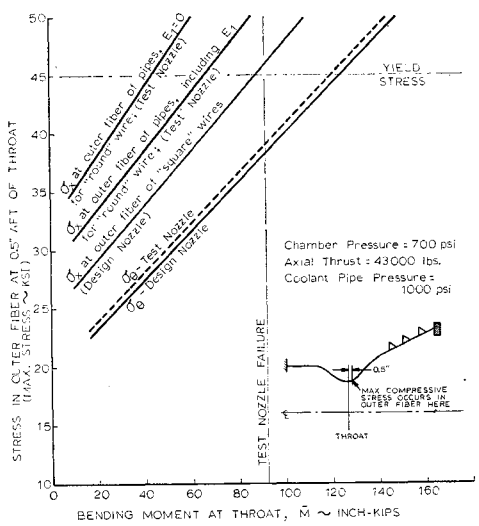

Fig. 10 Maximum compressive stress in nozzle wall as function of bending moment $\bar{M}$ at throat.

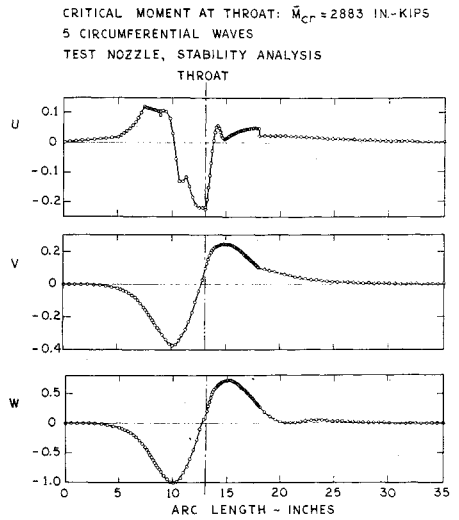

Fig. 11 Buckling mode for test nozzle.

nonsymmetric buckling modes are permitted. Hence, the loading must be modeled as axisymmetric. The appropriate load model consists of replacement of the lateral load S by an axial compressive load $V_B = 51S/(\pi r_t r_B)$, which gives the same maximum compressive load/length at the throat as that calculated through the assumption that the bending moment at the throat, $\bar{M} = 51S$, is reacted in the nozzle by an axial load which varies as $\cos\theta$.

The dotted lines in Fig. 9 show the results obtained with the test nozzle loaded only by $V_B = 51/(\pi r_t r_B) = 0.212$ lb/in. This axisymmetric load is equivalent in the sense just described to a lateral shear load $S = 1$ lb, to which the solid lines in Fig. 9 correspond. It is seen that in the throat region the axisymmetric load model is fairly accurate. Away from the throat the axisymmetric model is less accurate. Because the diameter of the nozzle changes, the axisymmetric load $V_B = 51/(\pi r_t r_B)$ is equivalent to $\bar{M} = 51S$ only at the throat. The normal displacement w is poorly approximated in the aft region (segments No. 5 and No. 6) because the almost rigid body displacement and rotation of this region is, of course, not present with the axisymmetric equivalent load, V_B.

The BOSOR3 program yields a buckling load $V_B = 12{,}000$ lb/in., corresponding to 5 circumferential waves. This load is equivalent to a lateral shear load $S = 56{,}000$ lb, or a bending moment at the throat $\bar{M} = 2883$ in.-kips. As seen from Fig. 10 this load is far above that corresponding to yielding of the wall material. The meridional distribution of the buckling mode is shown in Fig. 11. The design nozzle is predicted to buckle with three circumferential waves at $\bar{M} = 4715$ in.-kips, or $S = 92{,}500$ lb.

It is possible that the actual failure in the test was caused by general instability in the plastic regime, where the effective modulus of the wall material is greatly reduced. However, in the neighborhood of the yield stress (45,000 psi) the rate of change of modulus with stress is so great that it appears to be immaterial whether one defines failure as formation of a plastic hinge or general plastic instability. The associated predicted failure moment $\bar{M}$ would be about the same with either definition.

Summary and Conclusions

A computer analysis has been performed of two typical liquid-propellant rocket nozzles to determine maximum stress and stability limits corresponding to loads experienced by the nozzles during ignition and initial firing of the rocket engine. The dynamic loads are modeled as equivalent static loads, and comparisons are made between theoretical results and results from a static test. The failure load and mode from the test are reasonably well predicted by the theory, in which the nozzles are analyzed as symmetrically and nonsymmetrically loaded, layered orthotropic, longitudinally stiffened shells reinforced by rings treated as discrete structures. The theory reveals that there is a stress concentration near the throat which causes the material in the nozzle walls to fail at loads well below those corresponding to elastic buckling.

References

[1] Burnham, W. A., "Throat Bending Test of Titan III Second-Stage Chamber," Rept. 1389T, April 1966, Aerojet-General Corporation, Structural Test Lab.

[2] Bushnell, D., "Stress, Stability, and Vibration of Complex Shells of Revolution: Analysis and User's Manual for BOSOR3," N-5J-69-1, Sept. 1969, Lockheed Missiles & Space Company, Palo Alto, Calif.

[3] Cohen, G. A., "Computer Analysis of Asymmetric Buckling of Ring-Stiffened Orthotropic Shells of Revolution," *AIAA Journal*, Vol. 6, No. 1, Jan. 1968, pp. 141–149.

[4] Kalnins, A., "Analysis of Shells of Revolution Subjected to Symmetrical and Nonsymmetrical Loads," *Journal of Applied Mechanics*, Vol. 31, 1964, pp. 467–476.

[5] Percy, J. H., Pian, T. H. H., Klein, S., and Navaratna, D. R., "Application of Matrix Displacement Method to Linear Elastic Analysis of Shells of Revolution," *AIAA Journal*, Vol. 3, No. 11, Nov. 1965, pp. 2138–2145.

[6] Navaratna, D. R., Pian, T. H. H., and Witmer, E. A., "Analysis of Elastic Stability of Shells of Revolution by the Finite Element Method," *Proceedings AIAA/ASME 8th Structures, Structural Dynamics and Materials Conference*, March 1967, Palm Springs, Calif., pp. 175–183.

[7] Witmer, E. A., Pian, T. H. H., Mack, E. W., and Berg, B. A., "An Improved Discrete-Element Analysis and Program for the Linear-Elastic Static Analysis of Meridionally-Curved, Variable-Thickness, Branched Thin Shells of Revolution Subjected to General External Mechanical and Thermal Loads, Pt. 1: Analysis and Evaluation," ASRL TR 146-4, Pt. 1, SAMSO TR-68-310, Pt. 1, March 1968, MIT Aeroelastic and Structures Research Lab.

[8] Bushnell, D., Almroth, B. O., and Sobel, L. H., "Buckling of Shells of Revolution With Various Wall Constructions, Vol. 2, Basic Equations and Method of Solution," CR 1050, May 1968, NASA.

[9] Stein, M., "The Effect on the Buckling of Perfect Cylinders of Prebuckling Deformations and Stresses Induced by Edge Support," TN D-1510, Dec 1962, NASA.

[10] Budiansky, B. and Anderson, D. G. M., "Numerical Shell Analysis—Nodes Without Elements," *12th International Congress of Applied Mechanics*, Aug. 26–31, 1968, Stanford, Calif.

[11] Brogan, F. A. and Almroth, B. O., "Buckling of Cylinders With Cutouts," *AIAA Journal*, Vol. 8, No. 2, Feb. 1970, pp. 236–240.

[12] Bushnell, D., "Analysis of Buckling and Vibration of Ring-Stiffened, Shells of Revolution," *International Journal of Solids and Structures*, Vol. 6, No. 2, Feb. 1970, pp. 157–181.

[13] Williams, D., *Theory of Aircraft Structures*, Edward Arnold, London, 1960, Chap. 8, p. 279.

[14] Roark, R. J., *Formulas for Stress and Strain*, 3rd ed., McGraw-Hill, New York, 1954, p. 156.